Computing and Controlling the Compliance of a Robotic Hand

MARK R. CUTKOSKY AND IMIN KAO, STUDENT MEMBER, IEEE

Abstract—**Compliance is one of the most important quantities for characterizing the grasp of a robotic hand on a tool or workpiece. This is particularly true in fine manipulation (as in assembling components) where small motions and low velocities lead to dynamic equations that are dominated by compliance, friction, and contact conditions.**

In this paper we express the compliance of a grasp as a function of grasp geometry, contact conditions between the fingers and the grasped object, and mechanical properties of the fingers. We argue that the effects of structural compliance and small changes in the grasp geometry should be included in the computation. We then examine factors that can lead a grasp to become unstable, independently of whether it satisfies force closure. Finally, we examine the reverse problem of how to specify servo gains at the joints of a robotic hand so as to achieve, as nearly as possible, a desired overall grasp compliance. We show that coupling between the joints of different fingers is useful in this context.

NOMENCLATURE

$\delta \boldsymbol{x}_b$	Motion in the body coordinates.
$\delta \boldsymbol{x}_p$	Motion in the contact coordinates, $\delta \boldsymbol{x}_p = {}^{\mathrm{P}}_{\mathrm{B}}\boldsymbol{J}\delta \boldsymbol{x}_b$
$\delta \boldsymbol{x}_f$	Motion at the fingertip, $\delta \boldsymbol{x}_f = \boldsymbol{J}_\theta \delta\theta$.
$\delta \boldsymbol{x}_{\mathrm{tr}}$	Motion transmitted through the contact, $\boldsymbol{H}\delta \boldsymbol{x}_p = \boldsymbol{H}\delta \boldsymbol{x}_f = \delta \boldsymbol{x}_{\mathrm{tr}}$.
$\delta\theta$	Changes of joint angles.
$\boldsymbol{f}_b$	Force in the body coordinates.
$\boldsymbol{f}_p$	Grasp force at point P on the body.
$\boldsymbol{f}_f$	Grasp force at point F at the fingertip, $\boldsymbol{f}_f = \boldsymbol{f}_p$.
$\boldsymbol{f}_{\mathrm{tr}}$	Force transmitted through the contact, $\boldsymbol{f}_p = \boldsymbol{f}_f = \boldsymbol{H}^T \boldsymbol{f}_{\mathrm{tr}}$.
τ	Joint torques.
${}^{\mathrm{P}}_{\mathrm{B}}\boldsymbol{J}$	Coordinate transformation matrix, ${}^{\mathrm{P}}_{\mathrm{B}}\boldsymbol{J}\delta \boldsymbol{x}_b = \delta \boldsymbol{x}_p$.
$\boldsymbol{H}$	Contact constraint matrix.
$\boldsymbol{J}_\theta$	Joint Jacobian matrix, $\boldsymbol{J}_\theta \delta\theta = \delta \boldsymbol{x}_f$.
$\boldsymbol{D}$	Coordinate transformation matrix relating contact coordinates before and after infinitesimal motion.
${}^{\mathrm{P}}_{\mathrm{B}}\Delta \boldsymbol{J}_i^T$	${}^{\mathrm{P}}_{\mathrm{B}}\boldsymbol{J}^T(\boldsymbol{D}_i^T - \boldsymbol{I})$ that represents a differential Jacobian.
Ω	$\Omega = (\boldsymbol{H}\boldsymbol{C}_s\boldsymbol{H}^T - \boldsymbol{H}\boldsymbol{C}_s\boldsymbol{H}^T\boldsymbol{H}\boldsymbol{K}_p\boldsymbol{H}^T\boldsymbol{H}\boldsymbol{C}_s\boldsymbol{H}^T)$.
$\boldsymbol{B}$	$\boldsymbol{H}\boldsymbol{J}_\theta$.
${}^{\mathrm{P}}_{\mathrm{B}}\mathfrak{J}$	Concatenated coordinate transformation matrix.
$\mathfrak{K}$	Concatenated contact constraint matrix.
$\mathfrak{J}_\theta$	Concatenated joint Jacobian matrix.
$\boldsymbol{K}$	Stiffness, which is generally defined as $\partial f/\partial \boldsymbol{x}$ as in (1).
$\boldsymbol{K}_\theta$	The joint stiffness matrix, $\boldsymbol{K}_\theta = \boldsymbol{C}_\theta^{-1}$.
$\boldsymbol{K}_f$	The stiffness matrix in the fingertip coordinates, $\boldsymbol{K}_f = \boldsymbol{C}_f^{-1}$ if it is invertible.
$\boldsymbol{K}_b$	Stiffness matrix due to servo and structural compliance in the body coordinates.
$\boldsymbol{K}_J$	Stiffness matrix due to changes in geometry.
$\boldsymbol{K}_e$	Effective stiffness matrix, $\boldsymbol{K}_e = \boldsymbol{K}_b + \boldsymbol{K}_J$.
$\mathfrak{K}_p$	Concatenated stiffness matrix at contact points P.
$\mathfrak{K}_\theta$	Concatenated servo stiffness.
$\mathfrak{C}_\theta$	Concatenated servo compliance.
$\mathfrak{C}_s$	Concatenated structural compliance at the tip coordinates.
$\mathfrak{C}_f$	Concatenated fingertip compliance, $\mathfrak{C}_f = \mathfrak{J}_\theta \mathfrak{C}_\theta \mathfrak{J}_\theta^T + \mathfrak{C}_s$.
m_i	Number of joints for finger i.
n_i	Degrees of freedom at contact i.
nf	Number of fingers.
l	The Lagrange multipliers, $l = [\lambda_1 \lambda_2 \lambda_3 \cdots \lambda_n]$.
M_{ij}	Submatrices of the inverse of $\begin{bmatrix} \boldsymbol{K}_{f_i} & \boldsymbol{H}_i^T \\ \boldsymbol{H}_i & 0 \end{bmatrix}$ as derived in (20).
$B(x, y, z)$	Body coordinates.
$F(a, b, c)$	Contact coordinates at the contact point F on the fingertip.
$P(l, m, n)$	Contact coordinates at the contact point P on the body.
$O(x, y, z)$	World reference frame.
$\theta_1 \cdots \theta_m$	Joint angles of a finger.

Manuscript received October 10, 1987; revised June 2, 1988. This work was supported by the National Science Foundation under Grants DMC8552691 and DMC8602847, with additional support from the Standard Institute for Manufacturing and Automation.

The authors are with the Mechanical Engineering Department, Stanford University, Stanford, CA 94305-3030.

IEEE Log Number 8823936.

I. INTRODUCTION

THE EFFECTIVE compliance or stiffness of an object held in a robotic hand is an important quantity in tasks where forces and small motions are imparted to the object. For example, in assembling components it has been demonstrated that the chances of successful assembly are highest if the compliance matrix associated with the grasped part is diagonal at the point where the part first touches a mating component [15].

1042-296X/89/0400-0151$01.00

Similarly, in robotic grinding and deburring, the compliance matrix associated with the tool can be used to simplify the control problem [3]. The importance of compliance is also evident when examining the relative magnitudes of terms in the dynamic equations associated with fine motion tasks [12]. Low velocities and small relative motions lead to small inertia terms and a substantially linear analysis which is dominated by stiffness or its inverse, compliance.

In this paper we build upon recent grasp analyses by Salisbury [9], Kerr [7], Cutkosky [2], Kobayashi [8], and Nguyen [10], in which the instantaneous kinematics of multifingered hands have been defined in terms of Jacobian matrices and in which servo gains associated with the fingers contribute to the overall stiffness of the grip. As in [2], we are most interested in cases for which soft, anthropomorphic fingers are in contact with the object so that deformation and rolling of the fingertips cannot be ignored.

The first problem addressed in this paper is to obtain the effective compliance of an object held by a multifingered hand. In contrast to previous efforts, we assume that the fingers may be constructed from relatively flexible materials (such as molded thermoplastics) so that their structural compliance must be added to the compliance of the fingertips and to the controllable servo compliance of the joints. As Table II shows, even when fingers are made of aluminum, elasticity in the drive cables and in the joints produces significant compliance.

The effective compliance or stiffness of the grasped object depends not only on the compliances of the fingers but also on terms that arise from small changes in the grasp geometry as the object is perturbed by external forces. When grasp forces are large, these geometric terms may make the grasp statically unstable. In Section III we provide a new, systematic method for computing the matrix, $\boldsymbol{K}_J$, that represents these terms.

The overall grasp thickness matrix, containing structural, servo, and geometric terms, is a useful measure of the grasp. The rank and the eigenvalues of this matrix tell us about the mobility and stability of the grasp.[1] The relative magnitudes of the elements tell us how sensitive the grasp forces are to small motions in various directions. In addition, as discussed in [6], the grasp stiffness is useful in predicting the onset of sliding motion since it provides information about how rapidly the normal and tangential force components will change at each contact when the object is disturbed.

Finding the stiffness of a part grasped in a robotic hand is useful for predicting the grasp behavior and for discriminating among competing grasps when contemplating a task with particular requirements. For controls purposes, however, the reverse problem is of more interest: adjusting the servo gains at the finger joints so as to achieve a desired grasp stiffness. In many cases it is not possible to achieve exactly the required stiffness, but in Section IV we explore the methods that involve coupling the control of joints on different fingers to achieve a best approximation. The results of the forward and reverse compliance analysis are illustrated with several examples.

[1] In this paper we address only quasi-static stability, ignoring drive-train and actuator dynamics and the effects of rapidly varying, task- induced forces.

II. Previous Investigations of Grasp Compliance and Stiffness

Grasp compliance and stiffness have been studied by several investigators. The earliest analysis is that of Asada [1] in which a two-dimensional model of the object and the fingers leads to a potential function for describing stable grasps. The analysis assumes that fingers are essentially springs that move along a given locus with a single degree of freedom. Friction is ignored at the contacts between the fingers and the object and stable grasps are those for which the object will slide back to its initial equilibrium position after being displaced. The analysis gives intuitively satisfying results for handling slippery objects and where the main concern is that the object should not be dropped. However, in everyday manipulation tasks people and robots take advantage of friction. Consequently, subsequent grasp analyses have generally included friction at the contact points.

Salisbury [9] augments the resultant force and torque on the object with internal grasp forces so that an invertible 9×9 stiffness matrix is obtained for a three-fingered hand. The resulting stiffness matrix is useful for grasp control and simplifies programming the hand for certain manipulations. Cutkosky [2] examines the effective stiffness of a grasped object and shows that it is a function not only of the servo parameters but also of fingertip models and of small changes in the grasp geometry as the object is perturbed by external forces. Nguyen [10] addresses the stiffness and stability of planar and three-dimensional objects grasped by "virtual springs" corresponding to force components, or wrenches, at the finger/object contact points. Nguyen also proposes a least squares solution for specifying the stiffnesses of the "virtual springs" to obtain a desired grasp stiffness. However, he does not address the relation of "virtual springs" to joints of an actual hand. In this paper we consider a related problem: specifying the joint servoing in fingers with known structural properties to achieve a desired grasp compliance. The inclusion of the finger kinematics produces somewhat more complexity, but, due to coupling terms, also provides more opportunities for controlling the stiffness matrix.

III. Stiffness in Grasping

In its most general form, the stiffness of a grasp is a linearized expression of the relationships between forces applied to the grasp and the resulting motions

$$\boldsymbol{K} = \frac{\partial \boldsymbol{f}}{\partial \boldsymbol{x}}. \tag{1}$$

The resulting matrix can describe force/motion relationships both internal and external to the grasped object [9], but in this section we concern ourselves only with stiffness of the object with respect to external forces and moments.

As a partial derivative, the grasp stiffness permits us to look beyond instantaneous properties such as connectivity[2] and force-closure[3] and to examine the *sensitivity* of the grasp

[2] The connectivity of a grasp is the number of degrees of freedom between the grasped object and the palm of the hand [9].

[3] A grasp has force-closure if it can resist forces and moments from any direction, assuming the fingertips maintain contact with the object [11].

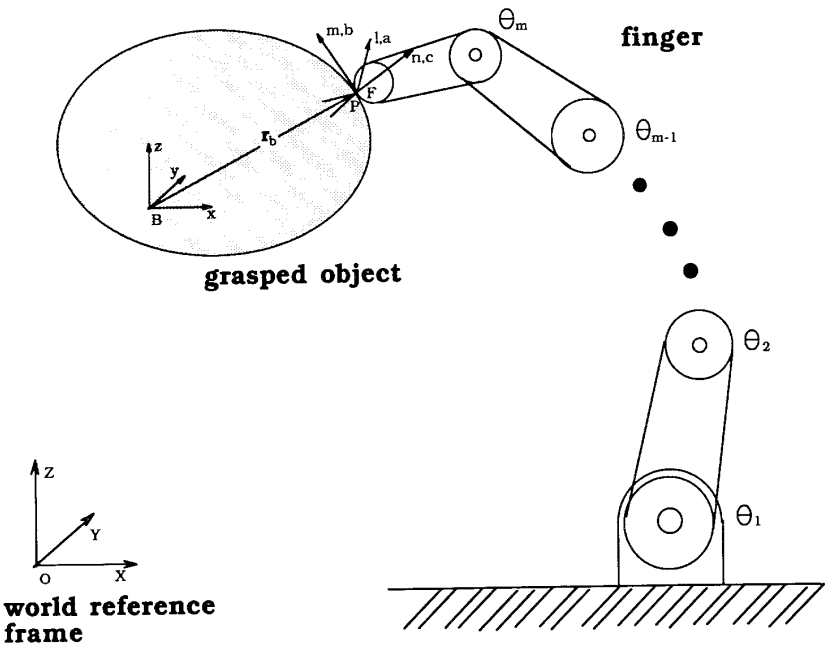

Fig. 1. Coordinate systems for a single finger touching a grasped object.

TABLE I
FORWARD FORCE/MOTION RELATIONSHIPS FOR FINGER AND OBJECT IN FIG. 1

motion	$J_\theta \delta\theta = \delta x_f$	$H\delta x_f = \delta x_{tr} = H\delta x_p$	${}^{P}_{B}J\delta x_b = \delta x_p$
	$(6 \times m)(m \times 1)(6 \times 1)$	$(n \times 6)(6 \times 1)(n \times 1)(n \times 6)(6 \times 1)$	$(6 \times 6)(6 \times 1)(6 \times 1)$
	JOINTS $\rightarrow$ $\leftarrow$	**CONTACT** $\leftarrow$ $\rightarrow$	**OBJECT**
force	$J_\theta^T f_f = \tau$	$f_f = H^T f_{tr} = f_p$	${}^{P}_{B}J^T f_p = f_b$
	$(m \times 6)(6 \times 1)(m \times 1)$	$(6 \times 1)(6 \times n)(n \times 1)(6 \times 1)$	$(6 \times 6)(6 \times 1)(6 \times 1)$

to disturbances. In fact, as Salisbury [9] points out, K is a direct measure of quasi-static grasp stability. As long as K is positive-definite, the changes in the forces on the object will have a stabilizing effect.

In the following subsections, we establish the force/motion relationships for the grasp and develop general expressions for the grasp stiffness in terms of finger compliances, contact types, and changes in the grasp geometry.

A. Forward Force/Motion Relationships

In this section we develop a framework for stiffness computation that includes the effects of

- servo compliance
- structural compliance
- changes in geometry
- coupling among different joints and fingers
- different contact types
- changes in contact location (e.g., due to rolling).

Fig. 1 shows the coordinate systems and Table I summarizes the forward force/motion relationships for a single finger touching an object. For derivations of the force/velocity transformations see [2], [7], [8]. In Table I, J_θ is the Jacobian matrix relating joint velocities to tip velocities in the $F(abc)$ coordinate system and ${}^{P}_{B}J$ is a Cartesian transformation matrix between the $B(xyz)$ coordinate system in the body and the $P(lmn)$ system at the contact point. At each contact, the force and velocity constraints are represented by an $n \times 6$ matrix H. Thus for a soft finger as defined by Salisbury [9]

$$H = \begin{bmatrix} 1 & 0 & 0 & 0 & 0 & 0 \\ 0 & 1 & 0 & 0 & 0 & 0 \\ 0 & 0 & 1 & 0 & 0 & 0 \\ 0 & 0 & 0 & 0 & 0 & 1 \end{bmatrix}.$$

The reciprocal force constraints at the contact can be derived from force equilibrium

$$f_p = f_f = H^T f_{tr}. \tag{2}$$

Thus for a point contact with friction $n = 3$, and the number of nonzero elements in f_p or f_b is three. In the following derivations we will also make use of the fact that H^T is the generalized inverse of H.

Concatenated Force/Motion Relationships: When several fingers like the finger in Fig. 1 grasp an object, the resulting configuration includes both serial and parallel kinematics. Each finger is a serial kinematic chain, while the combination

of several fingertips pressing against a single object forms a parallel mechanism. As a result, any attempt to compute the joint forces or motions needed to produce desired forces or motions of the object will involve both direct and inverse kinematic computations [7], and must accommodate static indeterminacy, redundancy, and over-constraint. In computing the grasp stiffness, we are subject to the same complications since we need to propagate motions from the object out to the finger joints and then propagate changes in the joint forces back to the object. However, as we shall see in the following section, the inclusion of structural compliances permits a systematic approach for arbitrary combinations of fingers, joints, and contact types. This is an important advantage since fingers are continually making and breaking contact with the object, and rolling or sliding from faces to edges, as the object is manipulated.

We concatenate ${}^{\mathrm{P}}_{\mathrm{B}}\boldsymbol{J}$, $\boldsymbol{H}$, and $\boldsymbol{J}_\theta$, so that we can simultaneously express the force/motion relationships for all the fingers of a grasp. The new equations have the same form as those in Table I

$$ {}^{\mathrm{F}}\mathfrak{J}_\theta \delta\theta = \delta \boldsymbol{x}_f \tag{3} $$

$$ ({}^{\mathrm{F}}\mathfrak{J}_\theta)^T \boldsymbol{f}_f = \tau \tag{4} $$

where τ and $\delta\theta$ are concatenated vectors of all the joint torques and infinitesimal joint motions and $\boldsymbol{f}_f$ and $\delta\boldsymbol{x}_f$ are concatenated vectors of forces and infinitesimal motions at the fingertips. The contact equations over all fingertips now become

$$ \mathfrak{K}\delta\boldsymbol{x}_p = \mathfrak{K}\delta\boldsymbol{x}_f \tag{5} $$

$$ \boldsymbol{f}_p = \boldsymbol{f}_f = \mathfrak{K}^T \boldsymbol{f}_{\mathrm{tr}}. \tag{6} $$

Finally, between the contact and the object $B(xyz)$ coordinate system we have

$$ \underset{(6\cdot nf\times 6)}{{}^{\mathrm{P}}_{\mathrm{B}}\mathfrak{J}} \quad \underset{(6\times 1)}{\delta\boldsymbol{x}_p} = \underset{(6\cdot nf\times 1)}{\delta\boldsymbol{x}_p} \tag{7} $$

and

$$ \underset{(6\times 6\cdot nf)}{({}^{\mathrm{P}}_{\mathrm{B}}\mathfrak{J})^T} \quad \underset{(6\cdot nf\times 1)}{\boldsymbol{f}_p} = \underset{(6\times 1)}{\boldsymbol{f}_b} \tag{8} $$

where ${}^{\mathrm{P}}_{\mathrm{B}}\mathfrak{J}$ is a $(6\cdot nf\times 6)$ matrix transforming infinitesimal motions $\delta\boldsymbol{x}_b$ of the object to equivalent motions at the contact.

B. Forward Stiffness Computation

We are now in a position to expand (1) by the chain rule, using (6) and (8)

$$ \frac{\partial \boldsymbol{f}_b}{\partial \boldsymbol{x}_b} = \frac{\partial({}^{\mathrm{P}}_{\mathrm{B}}\mathfrak{J}^T \boldsymbol{f}_f)}{\partial \boldsymbol{x}_b} = \underbrace{({}^{\mathrm{P}}_{\mathrm{B}}\mathfrak{J}^T)\frac{\partial \boldsymbol{f}_f}{\partial \boldsymbol{x}_b}}_{\boldsymbol{K}_b} + \underbrace{\frac{\partial({}^{\mathrm{P}}_{\mathrm{B}}\mathfrak{J}^T)\boldsymbol{f}_f}{\partial \boldsymbol{x}_b}}_{\boldsymbol{K}_J}. \tag{9} $$

The first part of the right-hand side of (9) expresses the restoring forces at the contacts resulting from the structural and servo stiffness of the fingers. The matrix associated with these terms is $\boldsymbol{K}_b$, and is derived in Section III-C. The second term $\boldsymbol{K}_J$ represents the effects of small changes in the grasp configuration. These terms become important when the grasp forces, $\boldsymbol{f}_f$, are large compared to the restoring forces. $\boldsymbol{K}_J$ is derived in Section III-D.

C. Computing $\boldsymbol{K}_b$: The Effects of Restoring Forces

In this subsection we derive expressions for the compliances of the fingers, beginning with the individual joint and structural compliances. We then impose the contact constraints and transform the fingertip stiffness matrix to the body coordinate frame to obtain the contribution of joint and structural compliances to the overall grasp stiffness.

As discussed in previous analyses [9], the joint stiffnesses $\mathcal{K}_{\theta_{ij}}$ are due, to first order, to position feedback gains in the fingers. Thus a single finger with m joint servos would produce an $m\times m$ joint stiffness matrix, which could be inverted to obtain a joint compliance matrix. Often, however, the fingers will be coupled. For example, the human hand exhibits both active (servo) and passive (structural) coupling among the fingers. If we wiggle our fourth fingers, it is nearly impossible to keep the third and fifth fingers from moving in sympathy. Therefore, we establish a concatenated joint compliance matrix

$$ \mathcal{C}_\theta = \mathcal{K}_\theta^{-1} = \begin{bmatrix} \boldsymbol{C}_{\theta_{11}} & \boldsymbol{C}_{\theta_{12}} & \cdots & \boldsymbol{C}_{\theta_{1,nf}} \\ \boldsymbol{C}_{\theta_{21}} & \boldsymbol{C}_{\theta_{22}} & \cdots & \boldsymbol{C}_{\theta_{2,nf}} \\ & & \ddots & \\ & \cdots & & \boldsymbol{C}_{\theta_{nf,nf}} \end{bmatrix}. \tag{10} $$

Applying (3) and (4) and using the principal of virtual work, we obtain an equivalent compliance matrix for the fingertips

$$ \mathcal{C}_j = \mathfrak{J}_\theta \mathcal{C}_\theta \mathfrak{J}_\theta^T. \tag{11} $$

If the fingers are not coupled, $\mathcal{C}_j$ is block-diagonal. More generally, $\mathcal{C}_j$ is a symmetric $(6\cdot nf\times 6\cdot nf)$ matrix (where nf is the number of fingers) but will be singular as long as the fingers have less than six joints.

To the controllable joint compliances we must add the uncontrollable structural compliance. In industrial grippers, structural compliance may be negligible but in dexterous hands, the use of actuating cables and soft gripping surfaces leads to significant compliance. In some cases, the compliance is easiest to determine experimentally, applying known loads and recording deflections. For example, in recent tests on the Stanford/JPL hand, we measured the typical compliances shown in Table II. These values were measured with the fingers extended. The combined structural compliance, at approximately 10^{-4} N/m, is roughly 10 percent of the minimum achievable servo compliance. In more anthropomorphic hands, with softer links and fingertips, we expect structural compliance to be correspondingly more important.

The structural compliance matrix varies considerably as a function of finger position, and the problem of computing it is similar to that of computing inertia matrices in robot dynamics. As in dynamics, one possibility is to interpolate among stored values corresponding to different configurations [13]. If the structural compliance is dominated by known flexibilities in the fingertips, links, or cables we can also express the compliance directly in terms of finger orientation. For example, if flexibility in the links is dominant, the structural

TABLE II
TYPICAL STRUCTURAL COMPLIANCES IN THE STANFORD/JPL HAND

Component	Compliance in m/N
Cable compliance	3.1×10^{-5}
Joint and link compliance	1.0×10^{-5}
Fingertip compliance	1.1×10^{-4}

compliance at each fingertip becomes

$$^{F}\boldsymbol{C}_s = \sum_{j=1}^{m} {}^{F}\boldsymbol{J}_{l_j} \boldsymbol{C}_{l_j} {}^{F}\boldsymbol{J}_{l_j}^{T} + \boldsymbol{C}_{\text{tip}} \tag{12}$$

where $^{F}\boldsymbol{J}_{l_j}$ is a 6×6 Jacobian relating a coordinate system in the jth link to the $F(abc)$ coordinate system at the fingertip. An example of $\boldsymbol{C}_{\text{tip}}$ is derived in [3] for "very soft" fingertips and $\boldsymbol{C}_{l_j}$ can be estimated from elementary beam theory [6]. In general, $^{F}\boldsymbol{C}_s$ is a nonsingular 6×6 symmetric matrix, although the terms in $^{F}\boldsymbol{C}_s$ may be small compared to those in $^{F}\boldsymbol{C}_j$.

The concatenated fingertip compliance matrix is obtained by summing the joint and structural compliances for each finger

$$\mathcal{C}_f = \mathcal{C}_j + \mathcal{C}_s. \tag{13}$$

If $\mathcal{C}_f$ is invertible, which it usually will be if $\mathcal{C}_s$ is not negligible, we can immediately obtain the concatenated fingertip stiffness matrix $\mathcal{K}_f$. However, as observed earlier, the contact matrices $\mathcal{H}$ "filter out" some of the motions of the fingertips. Hence not all elements of $\mathcal{K}_f$ will be experienced by the grasped object. Therefore, we use (5) and (6) to define a new stiffness matrix, $(\mathcal{H}\mathcal{C}_f\mathcal{H}^T)^{-1}$ that represents the finger stiffness components seen through the contacts. Then, applying (5) and (6) again, we can expand this stiffness to a (singular) $(nf \cdot n \times nf \cdot n)$ matrix for the contact points on the object

$$\mathcal{K}_p = \mathcal{H}^T(\mathcal{H}\mathcal{C}_f\mathcal{H}^T)^{-1}\mathcal{H}. \tag{14}$$

Note that if structural compliance is negligible, the product $(\mathcal{H}\mathcal{C}_f\mathcal{H}^T)^{-1}$ will still be invertible as long as the grasp is fully "manipulable," i.e., if the fingers can impart arbitrary motions to the object [9]. As discussed in [6], the expression for $\mathcal{K}_p$ is particularly useful for sliding analyses, as its partitions $\mathcal{K}_{p_{ij}}$ indicate the stiffnesses that the object "sees" at each contact point.

Finally, in terms of the $B(xyz)$ coordinate system of the object, we apply (7) and (8) to obtain

$$\boldsymbol{K}_b = {}^{P}_{B}\mathcal{J}^T \mathcal{K}_p {}^{P}_{B}\mathcal{J} \tag{15}$$

where $\boldsymbol{K}_b$ is a 6×6 matrix representing the stiffness of the grasped object, due to servo and structural terms.

D. Computing $\boldsymbol{K}_J$: The Effects of Changes in Geometry

When a grasped object is displaced slightly, two things happen which may affect the overall grasp stiffness and stability: the fingers shift slightly with respect to the object and, if the fingers roll or slide, the contact points move upon the object. To compute the effects of these changes in the grasp geometry we first need to find an expression for the complete motions of the fingertips.

The following results will be derived for a single finger, as in Fig. 1 and Table I, since the overall effect can be obtained simply by summing the contributions of all fingers

$$\boldsymbol{K}_J = \sum_{i=1}^{nf} \boldsymbol{K}_{J_i}. \tag{16}$$

From the contact velocity constraints in Table I, we can specify some, but not all, of the components of the fingertip motion when the object is displaced slightly. We need to make some assumptions about the fingertip control to determine the remaining components. One possibility is to assume that the fingertip orientation remains essentially fixed with respect to some global coordinate system [6]. For long, multijointed fingers with point contract, this is probably a reasonable assumption. A more general assumption is that like any underconstrained elastic mechanism, the grasp will adopt a configuration that minimizes its potential energy, subject to kinematic constraints. In this case we can solve for the motion of the fingertips using Lagrange multipliers. Since the grasp is initially at equilibrium, displacing the object will increase the potential energy

$$\Delta\text{p.e.} = \frac{1}{2}(\delta\boldsymbol{x}_f^T \mathcal{K}_f \delta\boldsymbol{x}_f) - \delta\boldsymbol{x}_f^T \boldsymbol{f}_f \tag{17}$$

where $\delta\boldsymbol{x}_f^T(-\boldsymbol{f}_f)$ represents work done against the initial grasp forces. To minimize Δp.e. subject to the constraint $\mathcal{H}(\delta\boldsymbol{x}_f - \delta\boldsymbol{x}_p) = 0$ in (5), we define the cost function c as

$$c = \Delta\text{p.e.} + \boldsymbol{l}^T\mathcal{H}(\delta\boldsymbol{x}_f - {}^{P}_{B}\mathcal{J}\,\delta\boldsymbol{x}_b) \tag{18}$$

where $\boldsymbol{l}$ is a vector of Lagrange multipliers. To find the optimal solution, we differentiate c with respect to $\delta\boldsymbol{x}_f$ and obtain

$$\mathcal{K}_f \delta\boldsymbol{x}_f + \mathcal{H}^T\boldsymbol{l} = \boldsymbol{f}_f. \tag{19}$$

Combining (5) and (19), we have (20). Note that the potential energy includes the combined structural and servo stiffness. The matrix equation with Lagrange multipliers can be expressed in fingertip coordinates:

$$\begin{bmatrix} \mathcal{K}_f & \mathcal{H}^T \\ \mathcal{H} & 0 \end{bmatrix} \begin{bmatrix} \delta\boldsymbol{x}_f \\ \boldsymbol{l} \end{bmatrix} = \begin{bmatrix} \boldsymbol{f}_f \\ \mathcal{H}\delta\boldsymbol{x}_p \end{bmatrix} \tag{20}$$

where $\boldsymbol{l} = [\lambda_1\, \lambda_2\, \lambda_3\, \cdots\, \lambda_n]$ are the Lagrange multipliers. If $\mathcal{K}_f$ cannot be obtained by inverting $\mathcal{C}_f$, due to negligible structural compliance, the equations can be solved in the finger joint space. Solving for $\delta\boldsymbol{x}_f$ (where $\delta\boldsymbol{x}_f$ is the concatenated vector of all fingertip motions), we obtain

$$\begin{bmatrix} \delta\boldsymbol{x}_f \\ \boldsymbol{l} \end{bmatrix} = \begin{bmatrix} \mathcal{K}_f & \mathcal{H}^T \\ \mathcal{H} & 0 \end{bmatrix}^{-1} \begin{bmatrix} \boldsymbol{f}_f \\ \mathcal{H}\delta\boldsymbol{x}_p \end{bmatrix}. \tag{21}$$

For particular contact types with decoupled servo stiffness, the partitions of the inverse matrix in (21) can be computed symbolically in terms of $\boldsymbol{C}_f$ for each finger. Appendix I shows the solution for $\delta\boldsymbol{x}_{f_i}$ (where $\delta\boldsymbol{x}_f$ is the motion of each fingertip) for the case of independent point contacts with friction, where $\mathcal{K}_f$ is block-diagonal.

While $\delta\boldsymbol{x}_{f_i}$ represents the absolute motion of a fingertip,

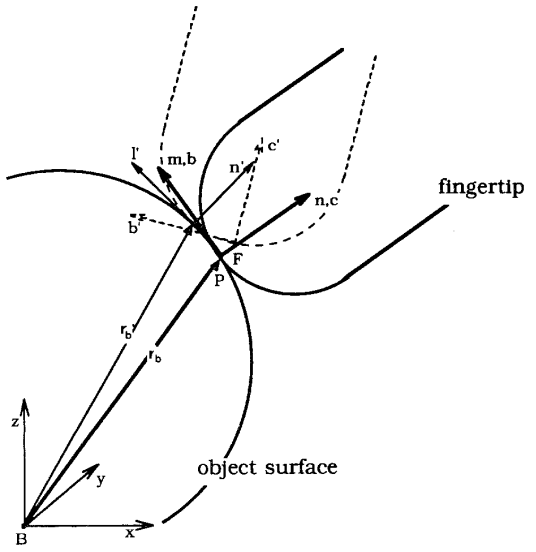

Fig. 2. Coordinate systems for a finger rolling on a grasped object.

$(\delta \boldsymbol{x}_{f_i} - \delta \boldsymbol{x}_{p_i})$ represents the relative motion of the fingertip with respect to the object. Expressed in the body coordinate frame $B(xyz)$, the relative motion becomes

$$ {}^{\mathrm{P}}_{\mathrm{B}}\boldsymbol{J}_i^{-1}(\delta \boldsymbol{x}_{p_i} - \delta \boldsymbol{x}_{f_i}) = \delta \boldsymbol{x}_b - {}^{\mathrm{P}}_{\mathrm{B}}\boldsymbol{J}_i^{-1}\delta \boldsymbol{x}_{f_i}. \tag{22} $$

By comparing $\delta \boldsymbol{x}_{f_i}$ and $\delta \boldsymbol{x}_{p_i}$, it is possible for a given contact geometry and contact type (e.g., rolling contact) to determine how the contact point is moving upon the object. Fig. 2 shows the contact coordinate systems before and after a fingertip has rolled slightly. The details of computing the motion of the contact can be complex, but solutions are discussed in [7] and [4] and, for the special case in which the finger does not twist about its own axis while rolling, a first-order approximation is given in [2]. For our purposes, it suffices to find the change in the resultant *force* on the object as the finger rotates with respect to the object and the contact point shifts upon the object. Put another way, from (6) we know that initially $\boldsymbol{f}_{p_i} = \boldsymbol{f}_{f_i}$, but after infinitesimal motion the force acting at the contact becomes

$$ \boldsymbol{f}'_{p_i} = \boldsymbol{D}_i^T \boldsymbol{f}_{f_i} \tag{23} $$

where $\boldsymbol{D}_i$ is a matrix describing a small, Cartesian transformation between the new position and orientation of the fingertip force $\boldsymbol{f}_{f_i}$ and the initial $P(lmn)$ contact coordinate system. Then, in body coordinates we have

$$ \boldsymbol{f}'_{b_i} = {}^{\mathrm{P}}_{\mathrm{B}}\boldsymbol{J}_i^T \boldsymbol{D}_i^T \boldsymbol{f}_{f_i} = {}^{\mathrm{P}}_{\mathrm{B}}\boldsymbol{J}_i^T \boldsymbol{f}_{f_i} + {}^{\mathrm{P}}_{\mathrm{B}}\Delta \boldsymbol{J}_i^T \boldsymbol{f}_{f_i}. \tag{24} $$

If no rolling or sliding occurs, $\boldsymbol{D}_i$ will contain only rotation terms, but in general both translations and rotations may be present. Solving for ${}^{\mathrm{P}}_{\mathrm{B}}\Delta \boldsymbol{J}_i^T$, we have

$$ {}^{\mathrm{P}}_{\mathrm{B}}\Delta \boldsymbol{J}_i^T = {}^{\mathrm{P}}_{\mathrm{B}}\boldsymbol{J}_i^T(\boldsymbol{D}_i^T - \boldsymbol{I}) \tag{25} $$

where ${}^{\mathrm{P}}_{\mathrm{B}}\Delta \boldsymbol{J}_i^T$ represents a differential Jacobian due to the changes in the geometry. Details are given in Appendix II.

Multiplying ${}^{\mathrm{P}}_{\mathrm{B}}\Delta \boldsymbol{J}_i^T$ by $\boldsymbol{f}_{f_i}$ gives us $\boldsymbol{K}_{J_i}$, that represents the change of forces due to geometry effects only. Since ${}^{\mathrm{P}}_{\mathrm{B}}\Delta \boldsymbol{J}^T$ can be expressed as a linear function of $\delta \boldsymbol{x}_b$, as shown in Appendix II, it is clear that ${}^{\mathrm{P}}_{\mathrm{B}}\Delta \boldsymbol{J}^T \boldsymbol{f}_f$ is a *linear* function of $\boldsymbol{f}_f$ and $\delta \boldsymbol{x}_b$ only. Since $\boldsymbol{f}_f$ is held constant in defining $\boldsymbol{K}_J$ in (9), the term ${}^{\mathrm{P}}_{\mathrm{B}}\Delta \boldsymbol{J}^T \boldsymbol{f}_f$ can be written as

$$ {}^{\mathrm{P}}_{\mathrm{B}}\Delta \boldsymbol{J}^T \boldsymbol{f}_f = \frac{\partial({}^{\mathrm{P}}_{\mathrm{B}}\Delta \boldsymbol{J}^T \boldsymbol{f}_f)}{\partial \delta \boldsymbol{x}_b}\, \delta \boldsymbol{x}_b. \tag{26} $$

Therefore, we obtain the stiffness matrix due to geometry changes as follows:

$$ \boldsymbol{K}_{J_i} = \frac{\partial({}^{\mathrm{P}}_{\mathrm{B}}\Delta \boldsymbol{J}_i^T \boldsymbol{f}_{f_i})}{\partial \delta \boldsymbol{x}_b}. \tag{27} $$

Finally, the effective grasp stiffness is obtained by summing $\boldsymbol{K}_b$ from Section III-C and $\boldsymbol{K}_{J_i}$ for all fingers

$$ \boldsymbol{K}_e = \boldsymbol{K}_b + \sum_{i=1}^{nf} \boldsymbol{K}_{J_i}. \tag{28} $$

E. Forward Procedure Examples

In the following examples we illustrate some of the issues that arise in computing the overall compliance of a grasp. To reduce the algebra, Example 1 illustrates a grasp with structural compliance but without changes in geometry and Example 2 illustrates the effects of changes in grasp geometry, without structural compliance.

Example 1: Inserting a Rivet into a Hole: Fig. 3 shows two three-joint fingers about to insert a small rivet into a chamfered hole. We wish to find $\boldsymbol{K}_b$ due to servo and structural compliance. The grasp is inspired by the thumb-index finger "pinch" that people use in precision tasks with tiny objects. The grasp also approximates a two-fingered grasp between the thumb and one of the fingers of the Stanford/JPL hand, except that the base axis of the thumb has been rotated parallel to the base axes of the fingers to simplify the Jacobian. Note that while the grasp appears planar in Fig. 3, it can manipulate the rivet along the x-axis, out of the plane of the page. For realism, we choose servo and structural compliances comparable to those listed for the Stanford/JPL hand in Table II and assume "very-soft" contacts between the fingertips and the rivet. The Jacobians and the compliance matrices are given in Appendix III-A. Applying (10)–(15), we arrive at the object stiffness matrix at the tip of the rivet

$$ \boldsymbol{K}_b = \begin{bmatrix} 2490 & 0 & 0 & 0 & 258 & 0 \\ 0 & 28900 & 0 & 191 & 0 & 0 \\ 0 & 0 & 61610 & 0 & 0 & 0 \\ 0 & 191 & 0 & 22 & 0 & 0 \\ 258 & 0 & 0 & 0 & 37 & 0 \\ 0 & 0 & 0 & 0 & 0 & 35 \end{bmatrix} $$

where the units are in newtons per meter and newton-meters for translational and rotational stiffness, respectively.

Discussion: Looking at $\boldsymbol{K}_b$, we notice that while the structural compliances are small compared to the servo compliances (about 10 percent), they prevent both the grasp and fingertip compliance matrices from becoming singular. By

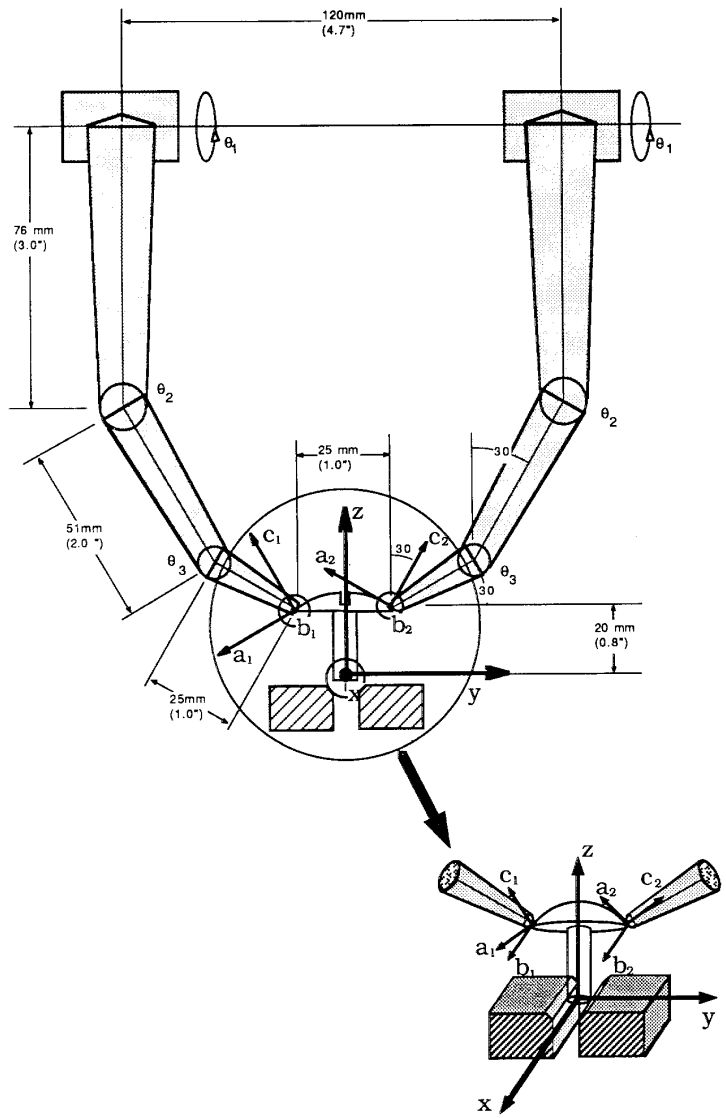

Fig. 3. Assembling a rivet with two soft-tipped fingers.

evaluating the eigenvalues of $\boldsymbol{K}_b$, we can readily find the stiffest and softest directions. The eigenvalues are all positive, confirming that $\boldsymbol{K}_b$ is stable. Also, since $\boldsymbol{K}_b$ has full rank, the grasp is a force-closure grasp and can resist forces and moments from any direction.[4] Finally, we observe that the stiffness matrix is decoupled in the z-direction since the grasp is symmetric about the z-axis. If $\boldsymbol{K}_b$ were completely diagonal, the center of compliance of the rivet would be at the $B(xyz)$ origin.

Before leaving this example, it is worth recalling that the stability and full rank properties of this grasp stem from our assumption of "very-soft" fingertips. In fact, the choice of contact model for an example such as this requires some care. The contact areas are small since the head of the rivet is thin. However, if we had assumed point contacts with friction, the change in $\mathfrak{IC}$ would result in a new stiffness matrix with a singular direction: $\vec{d} = [0\,0\,0\,0\,1\,0]$. In other words, the grasp could not resist moments about the y-axis and would not be a force-closure grasp—which seems unrealistic. A soft-finger model (in which the fingertips are free to roll about their a and b axes, but prevented from twisting about their c axes) seem more reasonable, but can also lead to an unrealistic stiffness matrix. Part of the problem is that the surface normal (the direction of the c-axis) is poorly defined at the edge of the rivet. In addition, the combination of a rotational constraint about the c-axis and a lack of constraint for rotations about the a and b axes, tends to produce a grasp stiffness matrix that is unrealistically stiff with respect to rotations about the z and y axes. As a result, the best model is the "very-soft" finger in which a full 6×6 compliance matrix exists for the contact, but for which rotational compliances are much larger than translational compliances, due to the small contact area. The

[4] However, this grasp cannot *impart* independent forces and motions in all directions, due to kinematic coupling.

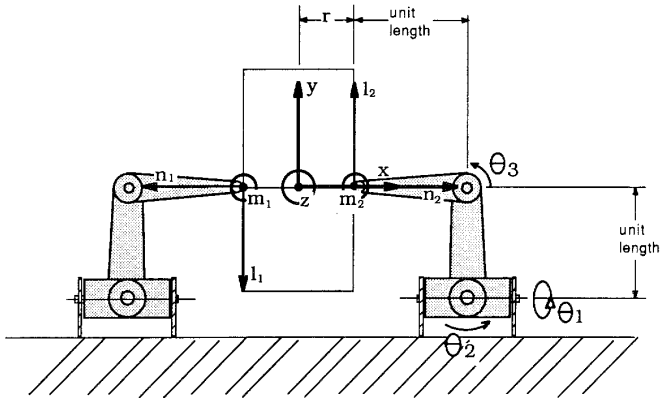

Fig. 4. A possible unstable grasp with point-contact fingers.

reader can also verify that this contact model is appropriate when grasping a small object such as a thumbtack between the thumb and index fingers, since the fingertips deform and may even partially enclose the edges of the object. As shown in [3], this model approaches the point-contact model in the limiting case as the contact area becomes small compared to the characteristic lengths of the fingertips or the object.

Example 2: The Effect of Changes in Grasp Geometry for Two Point-Contact Fingers: We wish to compute the effective stiffness, including the effects of changes in geometry, for the grasp shown in Fig. 4. As in Fig. 3, although the grasp looks planar, it can impart motions into and out of the page. For simplicity, we assume point-contact fingertips and negligible structural compliance. As a result, the grasp stiffness matrix $\boldsymbol{K}_b$ will be singular and we will not have a force-closure grasp. The Jacobians $\mathfrak{J}_\theta$ and ${}^{P}_{B}\mathfrak{J}$ and the joint stiffness matrix $\boldsymbol{K}_\theta$ are given in Appendix III-B. For a diagonal joint stiffness matrix, and the dimensions shown in Fig. 4, we apply (11), (14), and (15) to obtain

$$\boldsymbol{K}_b = 2\begin{bmatrix} (k_b + k_c) & 0 & 0 & 0 & 0 & -rk_c \\ 0 & k_c & 0 & 0 & 0 & 0 \\ 0 & 0 & k_a & 0 & 0 & 0 \\ 0 & 0 & 0 & 0 & 0 & 0 \\ 0 & 0 & 0 & 0 & r^2k_a & 0 \\ -rk_c & 0 & 0 & 0 & 0 & r^2k_c \end{bmatrix} \tag{29}$$

where r is one half the width of the object. (Because the links have unit length, the translational and rotational stiffness elements may appear to have inconsistent dimensions, but they are N/m and Nm, respectively.) As expected, $\boldsymbol{K}_b$ is singular and $\vec{y} = [0\,0\,0\,1\,0\,0]$ is the singular direction of the grasp.

We now wish to determine the effects of small changes in the grasp geometry. Following (16)–(27), we obtain $\boldsymbol{K}_J$

$$\boldsymbol{K}_J = 2\begin{bmatrix} 0 & 0 & 0 & 0 & 0 & 0 \\ 0 & -f_n & 0 & 0 & 0 & 0 \\ 0 & 0 & 0 & 0 & 0 & 0 \\ 0 & 0 & 0 & 0 & 0 & 0 \\ 0 & 0 & 0 & 0 & -rf_n & 0 \\ 0 & 0 & 0 & 0 & 0 & -rf_n(1 + r) \end{bmatrix} \tag{30}$$

where f_n represents the initial normal grasp force applied at the fingertips. As in $\boldsymbol{K}_b$, linear and rotational stiffness elements may appear to have the wrong dimensions, but this is an artifact of the unit link lengths. We observe that $\boldsymbol{K}_J$ is singular because the grasp geometry is unaffected by moving the object along the x-axis or rotating it about the x-axis. In addition, since the fingertips cannot rotate about their b-axes, there is no change in the grasp geometry for small motions in the z-direction. More importantly, the stiffness terms corresponding to rotations about the y and z axes are negative. Thus $\boldsymbol{K}_J$ tends to *destabilize* the grasp.

The effective grasp stiffness is obtained by adding $\boldsymbol{K}_b$ and $\boldsymbol{K}_J$ as in (28). The resulting expression for $\boldsymbol{K}_e$ makes intuitive sense

$$\boldsymbol{K}_e = 2\begin{bmatrix} (k_b + k_c) & 0 & 0 & 0 & 0 & -rk_c \\ 0 & (k_c - f_n) & 0 & 0 & 0 & 0 \\ 0 & 0 & k_a & 0 & 0 & 0 \\ 0 & 0 & 0 & 0 & 0 & 0 \\ 0 & 0 & 0 & 0 & r(rk_a - f_n) & 0 \\ -rk_c & 0 & 0 & 0 & 0 & r(rk_c - f_n - rf_n) \end{bmatrix} \tag{31}$$

Discussion: The effective stiffness matrix of this grasp reveals the important grasp properties. For example, since $\boldsymbol{K}_e$ is singular, we know that the grasp is not a force-closure grasp. Examination of the fourth row and column reveals that this is because the grasp cannot impart or resist moments about the x-axis. In addition, we find that if either

$$f_n \geq rk_a \quad \text{or} \quad f_n \geq \left(\frac{rk_c}{r+1}\right)\left(\frac{k_b}{k_b + k_c}\right)$$

$\boldsymbol{K}_e$ will not be positive-definite and the grasp will be unstable. We also see that for a given object size and finger stiffness, pressing harder without increasing the finger stiffness makes the grip less stable. This effect is easily demonstrated by pressing a small coin on edge between two fingers and gradually increasing the grasp force until the coin snaps over. In fact, since human muscles tend to become stiffer when larger forces are applied, there is some automatic compensation for this instability. If we purposefully tense our muscles, thereby increasing $\boldsymbol{K}_b$, we can preserve the positive definiteness of $\boldsymbol{K}_e$ for large grasp forces.

IV. Controlling the Grasp Stiffness

Given an initial grasp and a manipulation task, how should we control the finger joints so as to achieve a desired grasp stiffness?

Working backwards from (28), we have

$$\boldsymbol{K}_b = \boldsymbol{K}_e - \sum_{i=1}^{nf} \boldsymbol{K}_{J_i}$$

where $\boldsymbol{K}_e$ is the desired grasp stiffness and $\boldsymbol{K}_J$ is a function of the grasp geometry. There are then two major steps in the reverse procedure: 1) obtain $\mathcal{K}_p$ from the desired $\boldsymbol{K}_b$, and 2) obtain $\mathcal{C}_\theta$ or $\mathcal{K}_\theta$ from $\mathcal{K}_p$. We see from (14) and (15) that we can expand the contact stiffness as

$$\mathcal{K}_p = \begin{bmatrix} \boldsymbol{K}_{p_{11}} & \boldsymbol{K}_{p_{12}} & \cdots & \boldsymbol{K}_{p_{1,nf}} \\ \boldsymbol{K}_{p_{21}} & \boldsymbol{K}_{p_{22}} & \cdots & \boldsymbol{K}_{p_{2,nf}} \\ & & \ddots & \ddots \\ & \cdots & & \boldsymbol{K}_{p_{nf,nf}} \end{bmatrix} \tag{32}$$

where $\boldsymbol{K}_{p_{ij}}$ are the desired elements of $\mathcal{K}_p$ that we wish to specify. Note that for $i \neq j$, $\boldsymbol{K}_{p_{ij}}$ represent coupling terms among the joints on different fingers. These terms provide us with considerably more control over $\boldsymbol{K}_b$ than we could obtain from independently servoed fingers.

Equation (15) presents an underconstrained problem: there are many possible $\mathcal{K}_p$ that will satisfy $\boldsymbol{K}_b$. However, there are also numerous constraints on $\boldsymbol{K}_p$ imposed by the kinematics of the fingers, the contact types, and the joint configurations. The reverse compliance procedure is consequently difficult, often involving both overconstraint and underconstraint in a single grasp. The problem is similar to reverse force or velocity computations, for which solutions have been presented by Kerr [7] and Kobayashi [8], but is more complicated due to off-diagonal terms in the stiffness matrix and due to structural compliances. However, as we shall see in the following section, these extra terms also afford us more opportunities to achieve a desired grasp stiffness.

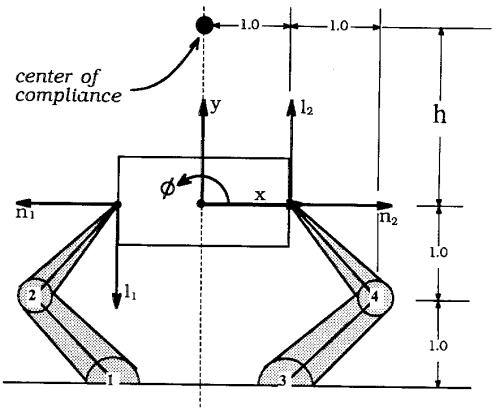

Fig. 5. Coordinates and center of compliance for a planar grasp.

Before launching into an exploration of general, three-dimensional reverse compliance it is worth examining a simple case that provides us with some physical insight for what can happen.

Example 3: Controlling the Compliance of a Planar Grasp: The dimensions and configuration of a simple, two-fingered grasp are shown in Fig. 5. Since that is a planar problem, forces and motions are represented by three-element vectors with two translational components and one rotation: $[x\ y,\ \phi]$. The left finger Jacobian is

$$\boldsymbol{J}_{\theta_1} = \begin{bmatrix} 0 & -1 \\ 2 & 1 \\ 1 & 1 \end{bmatrix} \tag{33}$$

which maps joints to the Cartesian coordinates $[l_1, n_1, \phi_{m_1}]$, and the right finger follows from symmetry. We will assume that structural compliance is confined to the fingertips and that the contact areas are small enough that the contact behaves nearly as a point contact. The symbolic $\mathcal{C}_\theta$, $\mathcal{K}$, and $\mathcal{C}_s$ matrices are given in Appendix III-C. If we keep the grasp symmetric, the forward and reverse compliance computations are simple enough to perform symbolically.

We want to locate the Center of Compliance of the object (the point for which the stiffness or compliance matrix becomes diagonal) at an arbitrary location, while also maintaining a stable (positive-definite) stiffness matrix and controlling the magnitude of the stiffnesses in the x, y, and ϕ directions. We examine four different cases, of increasing complexity:

1) no coupling in the control of the joints (stiffness matrix diagonal),
2) coupling only between the joints on each finger ($\mathcal{K}_\theta$ or $\mathcal{C}_\theta$ is block-diagonal),
3) full coupling among all joints,
4) an overconstrained case in which the lower right joint is locked.

In general, the planar graphs stiffness matrix $\boldsymbol{K}_b$ is a 3×3 symmetric matrix, resulting in six equations. However, since this grasp is symmetric, its stiffness will always be uncoupled

with respect to forces and motions along the centerline of the grasp, provided we control the joints symmetrically. In this case, there are only four equations to satisfy. For the $\mathcal{C}_\theta$, $\mathcal{JC}$, and $\mathcal{C}_s$ matrices in Appendix III-C, it can be shown that the location of the center of compliance with respect to the $B(xyz)$ origin is

$$h = \frac{C_{\theta_{24}} + C_{\theta_{22}} + 2C_{\theta_{14}} + 2C_{\theta_{12}}}{C_s + C_{\theta_{24}} + C_{\theta_{22}}} \tag{34}$$

where $C_{\theta_{ij}}$ are the elements of $\mathcal{C}_\theta = \mathcal{K}_\theta^{-1}$ in Appendix III-C, and are controlled by adjusting servo gains.

Case 1—no coupling: With no coupling, $\mathcal{C}_\theta$ is diagonal and $C_{\theta_{24}}$ and $C_{\theta_{12}}$ are zero so that

$$h = \frac{C_{\theta_{22}}}{C_s + C_{\theta_{22}}}.$$

As we might expect from examining the designs of Remote-Center-Compliance devices [15], [3], $h \to 0$ as the structural compliance becomes very large and $h \to 1$ when structural compliance is negligible. The latter case corresponds to the instantaneous center of rotation of a linkage formed by the fingers and object in Fig. 5. By adjusting the compliance of the second joints of the fingers we could, in theory, vary h between 0 and 1, except that there are practical upper and lower bounds on $C_{\theta_{22}}$. The lower bound is established by the maximum servo stiffness $(1/C_{\theta_{22}})$ that we can reasonably obtain while the upper bound is determined by the need to keep $\mathcal{C}_\theta$ positive-definite so that the grasp is stable.

Case 2—intra-finger coupling: If we allow coupling between the first and second joint of each finger we obtain another independent variable, $C_{\theta_{12}}$, that we can use in controlling $\boldsymbol{K}_b$ and h. The resulting expression for h is

$$h = \frac{C_{\theta_{22}} + 2C_{\theta_{12}}}{C_s + C_{\theta_{22}}}.$$

It would now appear that we could place the Center of Compliance anywhere along the centerline of the grasp except that again, we are limited by achievable upper bounds on the servo stiffnesses, and by the need to keep $\mathcal{C}_\theta$ positive-definite. If we look at the limiting case in which we are trying to maximize h (in which case C_s should approach zero), we arrive at the following bounds on h, in terms of the elements $\mathcal{C}_\theta$ to keep the joint compliance matrix positive-definite:

$$1 - 2\sqrt{\frac{n}{C_{\theta_{22}}} - 1} < h < 1 + 2\sqrt{\frac{n}{C_{\theta_{22}}} - 1} \tag{35}$$

where $n = (C_{\theta_{11}} + C_{\theta_{22}})$ is the trace of C_θ.

Case 3—inter- and intra-finger coupling: In contrast with the last two cases, if we permit coupling among the joints on different fingers, the expression for h is given by (34), from which it is clear that we now have considerably more freedom in controlling h while keeping $\mathcal{C}_\theta$ positive-definite by choosing appropriate off-diagonal terms.

Case 4—overconstraint: Suppose that the lower right joint is locked, so that we have a hand with just three joints. Can we still control $\boldsymbol{K}_b$? If we use coupling among all the joints, we have six independent variables, which would seem to be enough to control the six independent elements of $\boldsymbol{K}_b$ (the grasp is no longer symmetric). However, our intuition tells us that with only a single link on the right side, we will run into difficulties, since the tip of the link cannot move in the x direction without also moving in the y direction.

The symbolic expression for this nonsymmetric grasp matrix is complicated, but some special cases are worth examining. To begin with, we *must* have structural compliance to achieve any control of $\boldsymbol{K}_b$. In addition, if we try to diagonalize $\boldsymbol{K}_b$ at the origin we discover that this is only possible if the diagonal terms $k_{b_{11}}$ and $k_{b_{33}}$ (corresponding to stiffnesses in the x and ϕ directions, respectively) are also zero. More generally, it is possible to achieve a variety of $\boldsymbol{K}_b$ matrices, but our options are severely constrained. For example, if we try to place the center of compliance at a location [0 1 0] with the stiffnesses in the x, y, and ϕ directions of 50, 75, and 100, the resulting joint stiffness matrix

$$\boldsymbol{K}_\theta = \begin{bmatrix} -100 & 0 & 100 \\ 0 & 50 & -50 \\ 100 & -50 & 50 \end{bmatrix} \tag{36}$$

is not positive-definite.

This raises an interesting issue: How can we be sure that the reverse compliance procedure will not produce joint stiffness matrices with negative eigenvalues, and more importantly, how can we be sure that a positive-definite joint stiffness matrix will not produce an unstable $\boldsymbol{K}_b$ matrix? Fortunately, it can be shown that while a positive-definite $\boldsymbol{K}_b$ matrix does not always produce a positive-definite $\mathcal{K}_\theta$ matrix, the reverse is always true. The proof is given in Appendix IV. Thus a safe approach is to require that $\mathcal{K}_\theta$ be positive-definite and to use the off-diagonal terms resulting from coupling among the joints to increase the positive definiteness of $\mathcal{K}_\theta$.

A. A General Approach to the Reverse Procedure

The planar example in the last section has given us some idea of what to expect when solving for $\mathcal{K}_\theta$ to achieve a desired $\boldsymbol{K}_b$. The basic problem is to ensure that the limitations of the contacts and finger joints are reflected in $\mathcal{K}_p$.

We now proceed to elaborate the two steps of the reverse procedure. First, we have to find a matrix $\mathcal{K}_p$ that satisfies (15). As discussed previously, this is an underconstrained problem, and many solutions exist. However, $\mathcal{K}_p$ must also satisfy the following contact and joint constraints:

1) *Contact constraints:* $\mathcal{K}_p$ should reflect the constraints represented by $\mathcal{JC}$. In other words, $\mathcal{K}_p$ shoud have the same zero rows and columns as $\mathcal{JC}^T\mathcal{JC}$. This is because $\mathcal{K}_p = \mathcal{JC}^T(\mathcal{JC}\mathcal{C}_f\mathcal{JC}^T)^{-1}\mathcal{JC}$, as shown in (14).

2) *Joint constraints:* To ensure that the fingers can fully control the $\mathcal{K}_p$ matrix, we require that the nullspace of the product

$$\Omega = (\mathcal{C}_s' - \mathcal{C}_s'\mathcal{JC}\mathcal{K}_p\mathcal{JC}^T\mathcal{C}_s') \tag{37}$$

should be the same as the left nullspace of

$$\mathcal{B} = \mathcal{JC}\mathcal{J}_\theta. \tag{38}$$

The derivation is given in Appendix V. As an example, in the overconstrained case from Example 3, the finger tip on the

right is constrained to move in the $\pm[1\,1\,0]$ direction, which is orthogonal to the null space of Ω ($[1\ -1\ 0]$).

The remaining requirement, which surfaced in the overconstrained example in the last section is, that $\mathcal{C}_\theta$ should be kept positive-definite so that $\boldsymbol{K}_b$ will be positive-definite (or positive-semidefinite for a non-force-closure grasp). In addition, it may be useful to impose other restrictions for numerical or controls reasons.

Once we have found a suitable $\mathcal{K}_p$ matrix that satisfies the above constraints, it is straightforward to find $\mathcal{K}_\theta$. The presence of structural compliance provides some complication but, following the derivation in Appendix V, it can be shown that

$$\begin{aligned}\mathcal{K}_\theta = \mathcal{C}_\theta^{-1} &= [(\mathcal{J}\mathcal{C}\mathcal{J}_\theta)^*(\mathcal{C}'_s \\ &\quad - \mathcal{C}'_s\mathcal{J}\mathcal{C}\mathcal{K}_p\mathcal{J}\mathcal{C}^T\mathcal{C}'_s)(\mathcal{J}_\theta^T\mathcal{J}\mathcal{C}^T)^*]^{-1} \\ &\quad - (\mathcal{J}_\theta^T\mathcal{J}\mathcal{C}^T\mathcal{C}_s'^{-1}\mathcal{J}\mathcal{C}\mathcal{J}_\theta). \end{aligned} \tag{39}$$

Example 4: Reverse Compliance Computation for an Assembly Problem: We return to the three-dimensional grasp of Example 1, and attempt to determine appropriate joint stiffnesses so as to achieve a desired stiffness for the rivet. As Whitney [15] and others have demonstrated, it is ideal if the Center of Compliance of the rivet is placed at or near its tip. Therefore, we desire a stiffness matrix that will be diagonal at the $B(xyz)$ origin. In this example, we neglect the changes in geometry for small grasp forces, i.e., $\boldsymbol{K}_J$ is negligible. In addition, it is desirable for the stiffness along the x and y axes to be relatively small. We therefore specify the following desired grasp stiffness matrix

$$\boldsymbol{K}_e = \begin{bmatrix} 4000 & 0 & 0 & 0 & 0 & 0 \\ 0 & 10400 & 0 & 0 & 0 & 0 \\ 0 & 0 & 49000 & 0 & 0 & 0 \\ 0 & 0 & 0 & 0.1 & 0 & 0 \\ 0 & 0 & 0 & 0 & 14 & 0 \\ 0 & 0 & 0 & 0 & 0 & 27 \end{bmatrix}$$

where units are in N/m and Nm for linear and rotational stiffnesses.

Referring to (37) and (38), we construct a concatenated grasp stiffness matrix $\mathcal{K}_p$ that satisfies the criteria listed earlier in this section. The result is shown in Appendix III-D. Then, applying (39), we obtain $\mathcal{K}_\theta$

$$\mathcal{K}_\theta = \begin{bmatrix} 37.8 & 0 & 0 & -1.8 & 0 & 0 \\ 0 & 6.6 & -0.0006 & 0 & -3.5 & 3.2 \\ 0 & -0.0006 & 6.7 & 0 & 3.2 & -3 \\ -1.8 & 0 & 0 & 37.8 & 0 & 0 \\ 0 & -3.5 & 3.2 & 0 & 6.6 & -0.0006 \\ 0 & 3.2 & -3 & 0 & -0.0006 & 6.7 \end{bmatrix}$$

which can be checked through the forward procedure. The result is nearly identical to our desired $\boldsymbol{K}_b$ matrix (see Appendix III-D).

Discussion: As expected $\mathcal{K}_\theta$ is a symmetric 6×6 matrix which, like $\boldsymbol{K}_b$, has rank 6. In addition, although $\mathcal{K}_\theta$ is the concatenated stiffness matrix of two three-joint fingers, it is not block-diagonal. In other words, inter- and intra-finger coupling occurs to achieve the desired grasp stiffness.

Suppose that we do not permit coupling between the fingers? Then we cannot expect to achieve an arbitrary $\boldsymbol{K}_b$ matrix. The problem is that we have only two soft fingers, each with a 4×4 symmetric $\boldsymbol{K}_f$ matrix providing ten independent variables. Applying (15), we have

$$\boldsymbol{K}_b = {}^{\mathrm{P}}_{\mathrm{B}}\mathcal{J}^T\mathcal{K}_p\,{}^{\mathrm{P}}_{\mathrm{B}}\mathcal{J}$$

which yields up to 21 equations. Therefore, we have a problem with 21 equations for 20 unknowns. If we rewrite the equations in the form $\boldsymbol{Ax} = \boldsymbol{b}$, where $\boldsymbol{x}$ represents the free variables in matrices $\boldsymbol{K}_{p_i}$ and $\boldsymbol{A}$ and $\boldsymbol{b}$ are the known coefficients, the necessary and sufficient conditions for a solution to exist are

$$\det[\boldsymbol{A} \mid \boldsymbol{b}] \equiv 0 \qquad \text{and} \qquad \boldsymbol{i}_{21}^T\boldsymbol{y} \neq 0 \tag{40}$$

where $\boldsymbol{i}_{21}$ is a 21×1 unit vector, with the 21st element being 1, and $\boldsymbol{y}$ is a vector in the null space of augmented matrix $[\boldsymbol{A}\ \boldsymbol{b}]$. It can be further shown that there is no solution for this grasp if coupling is not allowed. More generally, Table III shows the *minimum* number of fingers required to fully specify the grasp stiffness for some common contact types.

V. Conclusions

The stiffness or compliance of a robotic grasp represents the rate of change of grasp forces with respect to small motions of the grasped object. The stiffness depends on structural compliances in the fingers and fingertips, on servo gains at the finger joints, and on small changes in the grasp geometry that affect the way in which the grasp forces act upon the object. As such, the grasp stiffness is a useful measure of the grasp. The rank of the stiffness matrix immediately reveals whether the grasp is a force-closure grasp and can resist forces and moments from arbitrary directions. The singular directions $\vec{d}$ are readily found through $\boldsymbol{K}_e\vec{d} = 0$. The eigenvalues of the matrix reveal the stiffest and softest directions. Generally, the stiffest directions will be those in which only structural compliance is present. Finally, the positive definiteness of the grasp matrix is a measrue of the quasi-static grasp stability. As discussed in Section III-D, an unstable grasp is one for which the contributions of changes in the grasp geometry $\boldsymbol{K}_J$ are significant, and negative.

For controlling a hand, we are interested in specifying servo gains at the finger joints for a desired grasp stiffness. For example, we may wish the grasp to have a center of compliance

TABLE III
MINIMUM NUMBER OF FINGERS NEEDED TO CONTROL K_e WITH AND WITHOUT COUPLING

Contact Type	No Coupling	Intra-Finger Coupling	Inter-Finger Coupling
Point contact without friction	21	21	6
Point contact with friction	7	4	2
Soft contact	6	3	2

at a particular point. Achieving the desired stiffness may be either an overconstrained or underconstrained problem, depending on the number of fingers and the number of joints per finger. One way to check this is to look at the stiffness matrix obtained through the forward procedure—it should have full rank and no extremely stiff directions.

Generally, it is useful to couple the servoing of joints on different fingers so that we can better control the off-diagonal terms of K_b. In the fourth example, we show that without inter-finger coupling we are not able to satisfy the compliance requirements of the task.

APPENDIX I

SYMBOLIC MATRIX INVERSE FOR POINT CONTACTS

If K_f is block-diagonal, we can treat each fingertip separately. If we divide the fingertip stiffness matrix in (20) into 3×3 partitions

$$K_{f_i} = \begin{bmatrix} K_{11} & K_{12} \\ K_{21} & K_{22} \end{bmatrix}.$$

Then, for point contacts, the inverse of the matrix in (21) can be expressed as

$$\begin{bmatrix} K_{f_i} & H_i^T \\ H_i & 0 \end{bmatrix}^{-1} = \begin{bmatrix} 0 & 0 & I_3 \\ 0 & K_{22}^{-1} & -K_{22}^{-1}K_{21} \\ I_3 & -K_{12}K_{22}^{-1} & (K_{12}K_{22}^{-1}K_{21} - K_{11}) \end{bmatrix}$$

where the matrix H_i is

$$H_i = \begin{bmatrix} 1 & 0 & 0 & 0 & 0 & 0 \\ 0 & 1 & 0 & 0 & 0 & 0 \\ 0 & 0 & 1 & 0 & 0 & 0 \end{bmatrix}$$

for point contact, and from (21), δx_{f_i} is simply

$$\delta x_{f_i} = \begin{bmatrix} H_i \delta x_{p_i} \\ -K_{22}^{-1}K_{21}H_i\delta x_{p_i} \end{bmatrix}$$

for point contacts. Similar symbolic expressions can be derived for soft contacts and very soft contacts. Thus the computation of δx_{f_i} need not be computationally expensive.

APPENDIX II

DIFFERENTIAL JACOBIAN

In (23) we define a 6×6 Cartesian transformation matrix between the initial $P(lmn)$ coordinate system and the new position and orientation of the grasp force after a small motion has taken place. If we denote the translation and rotation of the grasp force with respect to the initial $P(lmn)$ coordinate system as $\delta x = [dx, dy, dz, d\theta_x, d\theta_y, d\theta_z]$, we can express the Cartesian transformation as

$$D^T = \begin{bmatrix} \Delta A + I & | & 0 \\ \text{-------} & + & \text{----} \\ \Delta R(\Delta A + I) & | & \Delta A + I \end{bmatrix} \tag{41}$$

where ΔA^T and ΔR^T are small rotation and cross-product matrices, respectively. They can be generated from δx as

$$\Delta A^T = \begin{bmatrix} 0 & -d\theta_z & d\theta_y \\ d\theta_z & 0 & -d\theta_x \\ -d\theta_y & d\theta_x & 0 \end{bmatrix}$$

$$\Delta R^T = \begin{bmatrix} 0 & -dz & dy \\ dz & 0 & -dx \\ -dy & dx & 0 \end{bmatrix}.$$

If the orientation and the point of application of the grasp force do not change, A is simply an identity matrix and R a null matrix.

If we neglect second-order and smaller terms, we can express the differential Jacobian in (25) as

$${}^{P}_{B}\Delta J^T = \begin{bmatrix} \Delta A & | & 0 \\ \text{---} & + & \text{---} \\ \Delta R & | & \Delta A \end{bmatrix}. \tag{42}$$

APPENDIX III

EQUATIONS AND EXPRESSIONS IN EXAMPLES

A. Example 1

We assume servo stiffnesses comparable to those achievable in the Stanford/JPL hand and add some coupling among the joints on different fingers to achieve a typical joint stiffness matrix

$$\mathcal{K}_\theta = \mathcal{C}_\theta^{-1} = \begin{bmatrix} 10 & 0 & 0 & -1 & 0 & 0 \\ 0 & 5.65 & 0 & 0 & -1.5 & 0 \\ 0 & 0 & 3.66 & 0 & 0 & -1.1 \\ -1 & 0 & 0 & 10 & 0 & 0 \\ 0 & -1.5 & 0 & 0 & 5.65 & 0 \\ 0 & 0 & -1.1 & 0 & 0 & 3.1 \end{bmatrix}$$

where units are in Nm, for rotational stiffness. The joint Jacobian and the structural compliance matrix for the first finger

are

$$\boldsymbol{J}_{\theta_1} = \begin{bmatrix} 0 & -0.0728 & -0.022 \\ -0.1329 & 0 & 0 \\ 0 & 0.0127 & 0.0127 \\ -0.866 & 0 & 0 \\ 0 & 1 & 1 \\ -0.5 & 0 & 0 \end{bmatrix}$$

$$\boldsymbol{C}_{S_1} = \begin{bmatrix} 1.02 & 0 & -0.141 & 0 & -11.1 & 0 \\ 0 & 1.71 & 0 & 9.21 & 0 & 5.32 \\ -0.141 & 0 & 0.184 & 0 & 2.64 & 0 \\ 0 & 9.21 & 0 & 856 & 0 & 34.6 \\ -11.1 & 0 & 2.64 & 0 & 1008 & 0 \\ 0 & 5.32 & 0 & 34.6 & 0 & 520 \end{bmatrix} \times 10^{-4}.$$

The matrices for the second finger follow from symmetry. The structural compliance matrix was obtained by choosing values for the links comparable to those of the Stanford/JPL hand. A fingertip compliance matrix for a "very soft" finger was then added, with large rotational compliances in the l and m directions, corresponding to a small contact area and approaching the limiting case of a soft finger contact. For very soft fingertips, the contact matrix, $\mathcal{K}$, is a 12 × 12 identity matrix.

B. Example 2

We assume a diagonal joint stiffness matrix, with identical stiffnesses for both fingers

$$\mathcal{K}_\theta = \begin{bmatrix} k_a & 0 & 0 & 0 & 0 & 0 \\ 0 & k_b & 0 & 0 & 0 & 0 \\ 0 & 0 & k_c & 0 & 0 & 0 \\ 0 & 0 & 0 & k_a & 0 & 0 \\ 0 & 0 & 0 & 0 & k_b & 0 \\ 0 & 0 & 0 & 0 & 0 & k_c \end{bmatrix}.$$

The joint Jacobian and coordinate transformation matrix for the left finger are

$$\boldsymbol{J}_{\theta_1} = \begin{bmatrix} 0 & -1 & -1 \\ 1 & 0 & 0 \\ 0 & 1 & 0 \\ 0 & 0 & 0 \\ 0 & 1 & 1 \\ -1 & 0 & 0 \end{bmatrix}$$

$$\overset{P}{}_{B}\boldsymbol{J}_1 = \begin{bmatrix} 0 & -1 & 1 & 0 & 0 & r \\ 0 & 0 & 1 & 0 & r & 0 \\ -1 & 0 & 0 & 0 & 0 & 0 \\ 0 & 0 & 0 & 0 & -1 & 1 \\ 0 & 0 & 0 & 0 & 0 & 1 \\ 0 & 0 & 0 & -1 & 0 & 0 \end{bmatrix}.$$

The right finger follows from symmetry.

C. Example 3

In Example 3, the general servo stiffness matrix is

$$\mathcal{K}_\theta = \mathcal{C}_\theta^{-1} = \begin{bmatrix} K_{\theta_{11}} & K_{\theta_{12}} & K_{\theta_{13}} & K_{\theta_{14}} \\ K_{\theta_{12}} & K_{\theta_{22}} & K_{\theta_{23}} & K_{\theta_{24}} \\ K_{\theta_{13}} & K_{\theta_{23}} & K_{\theta_{33}} & K_{\theta_{34}} \\ K_{\theta_{14}} & K_{\theta_{24}} & K_{\theta_{34}} & K_{\theta_{44}} \end{bmatrix}$$

where the elements of $\mathcal{K}_\theta$ correspond to individual joint stiffnesses or coupling terms between different joints, as shown in Fig. 6. We also assume symmetry in this example so that $K_{\theta_{23}} = K_{\theta_{14}}$, $K_{\theta_{33}} = K_{\theta_{11}}$, $K_{\theta_{44}} = K_{\theta_{22}}$, and $K_{\theta_{34}} = K_{\theta_{12}}$. The structural compliance matrix is assumed to be diagonal (fingertip compliance only) so that

$$\mathcal{K}\mathcal{C}_s = \begin{bmatrix} C_s & 0 & 0 & 0 \\ 0 & C_s & 0 & 0 \\ 0 & 0 & C_s & 0 \\ 0 & 0 & 0 & C_s \end{bmatrix}.$$

D. Example 4

The null space vectors of Ω in this example are [0 3.760 −1 0 0 0] and [0 0 0 0 3.76 0 1] (in a, b, c, and rotation about c for each contact) which correspond to a single coupled motion in the object space, in which translation along the x-axis is unavoidably coupled with rotation about y.

If we take a $\boldsymbol{K}_p$ matrix that satisfies the constraints and apply the forward procedure, we obtain a $\boldsymbol{K}_b$ matrix that almost matches the desired $\boldsymbol{K}_b$ matrix. The only significant difference is due to the unavoidable coupling between x-axis translation and y-axis rotation:

$$\boldsymbol{K}_b' = \begin{bmatrix} 3530 & 0 & 0 & 0 & 142 & 0 \\ 0 & 10400 & 0 & 0 & 0 & 0 \\ 0 & 0 & 49000 & 0 & 0 & 0 \\ 0 & 0 & 0 & 0.1 & 0 & 0 \\ 142 & 0 & 0 & 0 & 14 & 0 \\ 0 & 0 & 0 & 0 & 0 & 27 \end{bmatrix}.$$

Appendix IV

Positive Definiteness of the Forward Procedure

We want to prove that a positive-definite $\mathcal{K}_\theta$ or $\mathcal{C}_\theta$ will result in a positive-semidefinite $\boldsymbol{K}_b$. We begin by recalling the "Law

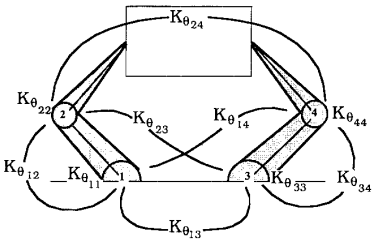

Fig. 6. Correlation between elements of K_θ and coupled joint control.

of Inertia" for a congruence transformation:

Law of Inertia: If the transformation matrix T in the congreuence transformation T^TQT is nonsingular, the signs of the eigenvalues are preserved [14]. Therefore, we have the following two theorems:

Theorem 1: If Q is positive-definite, its congruence transformation is positive-semidefinite, i.e.,

$$\forall Q > 0 \Rightarrow T^TQT \geq 0, \qquad \text{for any matrix } T$$

also

$$Q > 0 \Rightarrow T^TQT > 0, \qquad \text{when } \mathfrak{N}(T) = \{\ \}$$

where $\mathfrak{N}(T)$ is the null space of matrix T.

Proof: To prove the positive definiteness of T^TQT, we pre- and post-multiply by a vector x^T and x. Therefore

$$x^T(T^TQT)x = y^TQy$$

where $y = Tx$ is a vector. Clearly, from definition of positive definiteness, $y^TQy > 0$ if $y = Tx$ is nontrivial. That is, if $y \notin \mathfrak{N}(T)$ then $T^TQT > 0$; otherwise, $T^TQT \geq 0$. ■

Theorem 2: If $\mathcal{C}_\theta$ or $\mathcal{K}_\theta$ is positive-definite, then $\mathcal{K}_b$ obtained in the forward procedure will be positive-semidefinite. If the grasp is force-closure, then $\mathcal{K}_b$ is positive-definite.

Proof: If we begin with a positive-definite $\mathcal{C}_\theta$, then $\mathcal{C}_j$ in (11) is positive-semidefinite according Theorem 1. Since $\mathcal{C}_s$ is always positive-definite, $\mathcal{C}_f$ in (13) is positive-definite. Therefore, $\mathcal{J}\mathcal{C}_f\mathcal{J}^T$ is positive-definite from Theorem 1, as is its inverse. $\mathcal{K}_p$ and K_b in (15) are therefore positive-semidefinite. The stiffness matrix K_b is thus positive-semidefinite. If the grasp is force-closure then K_b is nonsingular and therefore positive-definite. ■

Appendix V

Obtaining Joint Stiffness in the Reverse Procedure

In this Appendix, we find the expression for the joint stiffness matrix K_θ in terms of the structural compliance and the desired K_p matrix. Note that all matrices discussed here can be the concatenated matrices for generalization. First, we use (11) and (13) to expand the product $(HC_fH^T)^{-1}$

$$(HC_fH^T)^{-1} = (HC_sH^T + HJ_\theta C_\theta J_\theta^T H^T)^{-1}.$$

Then, we use the standard matrix inverse formula [5]

$$(A + BCD)^{-1} = A^{-1} - A^{-1}B(DA^{-1}B + C^{-1})^{-1}DA^{-1}$$

(where A and C are nonsingular square matrices) to expand (14) as

$$K_p = H^TC_s'^{-1}H - H^TC_s'^{-1}B(B^TC_s'^{-1}B + C_\theta^{-1})^{-1}BC_s'^{-1}H \tag{43}$$

where $C_s' = HC_sH^T$ represents structural compliance seen by the object through contact, and $B = HJ_\theta$, such that $\delta x_{tr} = B\delta\theta$.

We wish to invert the relationship in (43) to obtain C_θ^{-1} in terms of K_p and C_s'. As a first step

$$K_p - H^TC_s'^{-1}H = -H^TC_s'^{-1}B(B^TC_s'^{-1}B + C_\theta^{-1})^{-1}B^TC_s'^{-1}H.$$

All the matrix products in the above equation have the same form, with rows and columns of zeros determined by the contact matrix H. Therefore, it makes no difference if we only consider only the nontrivial submatrices, that is, if we pre- and post-multiply by H, and H^T. Then since $HH^T = I$, and $n \times n$ identity matrix

$$(C_s' - C'_sHK_pH^TC'_s) = B(B^TC_s'^{-1}B + C_\theta^{-1})^{-1}B^T. \tag{44}$$

Now, since $B = HJ_\theta$ is usually not square, there are two possibilities.

I: If $m \leq n$, then $B^*B = I_m$ and

$$C_\theta^{-1} = K_\theta = [B^*(C_s' - C'_sHK_pH^TC_s')B^{T*}]^{-1} - (B^TC_s'^{-1}B) \tag{45}$$

where the superscript * stands for generalized inverse and I_m is an $m \times m$ identity matrix.

II: If $m > n$, the finger has redundant joints and the optimal solution can be obtained from generalized inverse of B by minimizing the norm of C_θ in which case (45) for C_θ still holds.

Ω in the Reverse Procedure: In the reverse procedure, we require that the desired matrix K_p be chosen such that product $\Omega = (C_s' - C_s'HK_pH^TC_s')$ has the same null space as B. Ω represents the coupled directions, as seen through the contacts, of the motions of the fingers.

Theorem: The null space of matrix Ω is the same as that of B, which is independent of the structural compliance, $\mathcal{C}_s$ and of $\mathcal{C}_\theta$, as long as $\mathcal{C}_\theta$ is positive-definite.

Proof: Substituting K_p from (14) into Ω and expanding, we obtain:

$$\Omega = C_s' - C_s'HH^T(BC_\theta B^T + C_s')^{-1}HH^TC_s'$$

$$= C_s' - C_s'[C_s'^{-1} - C_s'^{-1}B(B^TC_s'^{-1}B + C_\theta^{-1})^{-1}B^TC_s'^{-1}]C_s'$$

or

$$\Omega = B(B^TC_s'^{-1}B + C_\theta^{-1})^{-1}B^T. \tag{46}$$

Since $\mathcal{C}_s$ is always positive-definite, if we choose a positive-definite C_θ matrix then $(B^TC_s'^{-1}B + C_\theta^{-1})$ will be positive-

definite along with its inverse. From the theorem and proof in Appendix IV, we conclude that Ω has the same null space as $\boldsymbol{B}^T$ or the same left null space as $\boldsymbol{B}$, which is independent of the values of $\boldsymbol{C}_s$ and $\boldsymbol{C}_\theta$.

■

ACKNOWLEDGMENT

The authors wish to thank P. Akella, and R. Howe for their comments and their help in doing the experiments on the Stanford/JPL hand. They also wish to thank M. Nagurka and J. Jourdain at CMU for many useful discussions. Finally, they thank the reviewers for the excellent suggestions on the draft.

REFERENCES

[1] H. Asada, "Studies on prehension and handling by robot hands with elastic fingers," Ph.D. dissertation, Kyoto University, Kyoto, Japan, Apr. 1979.

[2] M. R. Cutkosky, *Robotic Grasping and Fine Manipulation.* Boston, MA: Kluwer, 1985.

[3] M. R. Cutkosky and P. K. Wright, "Active control of a compliant wrist in manufacturing tasks," *ASME J. Eng. for Ind.,* vol. 108, no. 1, pp. 36–43, 1985.

[4] Z. Ji, "Dexterous hand: Optimizing grasp by design and planning," Ph.D. dissertation, Stanford University, Stanford, CA, 1987.

[5] T. Kailath, *Linear Systems.* Englewood Cliffs, NJ: Prentice-Hall, 1st ed., 1980.

[6] I. Kao and M. Cutkosky, "Effective stiffness and compliance, and their application to sliding analysis," Tech. Rep. SIMA, Stanford University, Stanford, CA, Mar. 1987.

[7] J. Kerr, "Analysis of multifingered hands," Ph.D. dissertation, Stanford University, Stanford, CA, 1986.

[8] H. Kobayashi, "Control and geometrical considerations for an articulated robot hand," *Robotics Res.,* vol. 4, no. 1, pp. 3–12, 1985.

[9] M. T. Mason and J. K. Salisbury, *Robot Hands and the Mechanics of Manipulation* Cambridge, MA: MIT Press, 1985.

[10] V. Nguyen, "Constructuring force-closure grasps in 3-d," in *Proc. 1987 IEEE Conf. on Robotics and Automation,* pp. 240–245, Mar. 1987.

[11] M. Ohwovoriole, "An extension to screw theory and its applications to the automation of industrial assemblies," Ph.D. dissertation, Stanford University, Stanford, CA, Apr. 1980.

[12] M. A. Peshkin, "Planning robotic manipulation strategies for sliding objects," Ph.D. dissertation, Carnegie Mellon University, Pittsburgh, PA, 1986.

[13] M. H. Raibert and B. K. P. Horn, "Manipulator control using the configuration space method," *Industrial Robot (UK),* vol. 5, no. 2, pp. 69–73, June 1978.

[14] G. Strang, *Lienar Algebra and Its Applications.* New York, NY: Academic Press, 2nd ed., 1980.

[15] D. E. Whitney, "Part mating theory for compliant parts," First. Rep. The Charles Stark Draper Lab., Inc. Aug. 1980, NSF Grant DAR79-10341.

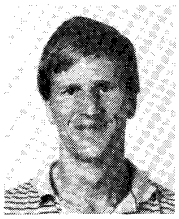

Mark R. Cutkosky received the Ph.D. degree from Carnegie-Mellon University, Pittsburgh, PA.

He was a Lecturer and research associate at Carnegie-Mellon University, where he also conducted research in the Robotics Institute. His research included programmable fixtures for manufacturing systems, grippers, sensors, and control schemes for robotic forging and machining cells, and grasping and fine manipulation in automated manufacturing. During this time he was also a design engineer at ALCOA. He joined the Design Division of the Mechanical Engineering Department at Stanford University, Stanford, CA, as an Assistant Professor in August 1985. He teaches courses in engineering design, mechanical systems, robotics, flexible manufacturing automation, and design for manufacturability. His research areas include robotics (particularly dexterous hands and tactile sensing) and the application of artificial intelligence to "concurrent product and process design" for mechanical parts and assemblies. He is an NSF Presidential Young Investigator.

Dr. Cutkosky is a member of ASME, SME, and Sigma Xi.

Imin Kao (S'87) was born in Tainan, Taiwan, in April 1960. He received the B.S. degree from National Chung Hsing University, Taichung, Taiwan in 1981 (with honors) and the M.S. degree from Stanford University, Stanford, CA, in 1985, both in mechanical engineering. He is currently a Ph.D. candidate in the Design Division of the Mechanical Engineering Department, Stanford University.

His research interests include robotics, manipulation, grasping and sliding analysis, and control.